
BiSup: Bidirectional Quantization Error Suppression for Large Language Models

Minghui Zou

College of Intelligence and Computing
Tianjin University
minghuizou@tju.edu.cn

Ronghui Guo

College of Intelligence and Computing
Tianjin University
ronghui_guo@tju.edu.cn

Sai Zhang

College of Intelligence and Computing
Tianjin University
zhang_sai@tju.edu.cn

Xiaowang Zhang

College of Intelligence and Computing
Tianjin University
xiaowangzhang@tju.edu.cn

Zhiyong Feng*

College of Intelligence and Computing
Tianjin University
zyfeng@tju.edu.cn

Abstract

As the size and context length of Large Language Models (LLMs) grow, weight-activation quantization has emerged as a crucial technique for efficient deployment of LLMs. Compared to weight-only quantization, weight-activation quantization presents greater challenges due to the presence of outliers in activations. Existing methods have made significant progress by exploring mixed-precision quantization and outlier suppression. However, these methods primarily focus on optimizing the results of single matrix multiplication, neglecting the bidirectional propagation of quantization errors in LLMs. Specifically, errors accumulate vertically within the same token through layers, and diffuse horizontally across different tokens due to self-attention mechanisms. To address this issue, we introduce BiSup, a **B**idirectional quantization error **S**uppression method. By constructing appropriate optimizable parameter spaces, BiSup utilizes a small amount of data for quantization-aware parameter-efficient fine-tuning to suppress the error vertical accumulation. Besides, BiSup employs prompt mixed-precision quantization strategy, which preserves high precision for the key-value cache of system prompts, to mitigate the error horizontal diffusion. Extensive experiments on Llama and Qwen families demonstrate that BiSup can improve performance over two state-of-the-art methods (the average WikiText2 perplexity decreases from 13.26 to 9.41 for Atom and from 14.33 to 7.85 for QuaRot under the W3A3-g128 configuration), further facilitating the practical applications of low-bit weight-activation quantization.

1 Introduction

The emergence and development of large language models (LLMs) have had a disruptive impact across various domains. Empirical evidence indicates that, compared to previous pre-trained language models (PLMs), LLMs can demonstrate powerful emergent capabilities when their scale reaches a

*Corresponding Author

certain threshold, thereby better adapting to complex real-world applications (Zhao et al., 2023a). However, the growth in model size is accompanied by an increase in the computational resources required for model deployment and inference, limiting the widespread application of LLMs in various resource-constrained scenarios, such as the edge.

To reduce the deployment and inference costs of models, model quantization has emerged as a promising approach (Nagel et al., 2021; Zhu et al., 2023; Wang et al., 2024). LLMs are typically trained and stored at high precision (e.g., FP16 or BF16). The objective of model quantization is to convert them into lower precision (e.g., INT4), thereby significantly reducing memory consumption while leveraging hardware features to accelerate inference speed. Model quantization comprises two main directions: Quantization-Aware Training (QAT) and Post-Training Quantization (PTQ). Compared to QAT methods, which require substantial data and computational resources, PTQ methods are widely used in practical applications owing to their low cost and high yield. From the perspective of quantized objects, model quantization encompasses two primary branches: weight-only quantization and weight-activation quantization. The weight-only quantization methods have been applied in various inference frameworks (Frantar et al., 2022; Lin et al., 2023). Nonetheless, as the model sizes and context lengths expand, the proportion of memory consumption attributed to activations escalates, thus rendering activation quantization a critical research issue.

Compared to weight-only quantization, weight-activation quantization poses greater challenges due to the presence of outliers in activations. A recognized finding is that while outliers are difficult to be quantized, they typically occur only in a few specific channels (Dettmers et al., 2022). Accordingly, existing methods are mainly investigated in two directions: mixed-precision quantization (Dettmers et al., 2022; Guo et al., 2023; Ashkboos et al., 2023) and outlier suppression (Xiao et al., 2023; Shao et al., 2023; Ma et al., 2024). The core idea of mixed-precision quantization methods lies in retaining a minority of outlier channels at high precision while quantizing the majority of normal channels to low precision. LLM.int8() (Dettmers et al., 2022) identifies outlier channels based on the magnitude of activations and then decomposes the weight matrix and activation matrix by channel. While the outlier matrices are multiplied at high precision, the normal matrices are first quantized to low precision. Building upon LLM.int8(), QUIK (Ashkboos et al., 2023) proposes improvements by replacing the RTN algorithm with the GPTQ (Frantar et al., 2022) and moving high-precision outlier channels to the end to compensate for quantization losses. Outlier suppression methods are grounded on the premise that, compared to activations, weights exhibit a smoother distribution and better quantization properties. Therefore, by means of equivalent transformations, outliers in activations can be transferred to weights to reduce the difficulty of activation quantization. SmoothQuant (Xiao et al., 2023) proposes an empirical formula to calculate a scaling factor based on the maximum values of activations and weights. OmniQuant (Shao et al., 2023) suggests that manually designed rules for offsetting and scaling outlier channels may not achieve optimal results, thus using gradient optimization methods as an alternative. AffineQuant (Ma et al., 2024) proposes an equivalent affine transformation, unifying previous equivalent transformation methods, and introduces a new optimization algorithm to ensure the reversibility of the transformation matrix.

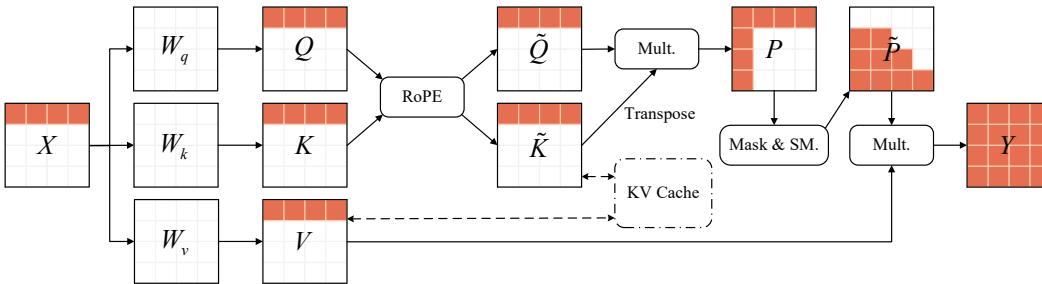


Figure 1: The error propagation within attention block under activation-only quantization. Different colors on the tensor represent different meanings, where orange indicates that it contains quantization error and white the opposite.

While existing methods have made significant progress in mitigating the effects of outliers, they primarily focus on optimizing the results of single matrix multiplication, neglecting the bidirectional

propagation of quantization errors in the model. This includes the error vertical accumulation within the same token through layers and the error horizontal diffusion between different tokens due to self-attention mechanisms. For convenience, we consider the error propagation within attention block under activation-only quantization, as illustrated in Figure 1. Within the block, there are consecutive matrix multiplications necessitating corresponding quantization and dequantization operations. The error introduced by the preceding quantized matrix multiplication influences the subsequent one, leading to error accumulation. Besides, because self-attention mechanisms involve interactions between different tokens, quantization errors appearing on one token will diffuse to other tokens, further contributing to a wider range of error vertical accumulation and resulting in a vicious cycle. Consequently, effectively suppressing bidirectional error propagation inside the model is a crucial step to ensure the effectiveness of existing high-performance quantization methods.

In this paper, we introduce BiSup, a **B**idirectional quantization error **S**uppression method. To alleviate the error vertical accumulation, it is required to minimize the quantization error of single matrix multiplication while counteracting the existing quantization error in time. Inspired by OmniQuant (Shao et al., 2023) and QLoRA (Dettmers et al., 2024; Liao and Monz, 2024), BiSup starts from the weight-activation quantization formula, considers the distribution pattern of activation outliers and the convergence of few-shot fine-tuning to design optimizable parameter spaces that require only a small amount of data and computational resources for calibration. To mitigate error horizontal diffusion, it is advantageous to preserve the accuracy of important tokens (i.e., tokens with larger attention weights). Analyzing the attention maps of LLMs, we notice that LLMs have a strong dependence on the first token. From the perspective of system prompt caching, BiSup introduces the prompt mixed-precision quantization strategy. By keeping a small amount of system prompt cache at high precision, the error of important token interactions can be effectively minimized. Our contributions are as follows:

- We indicate the bidirectional propagation of quantization errors, providing a new research perspective for post-training quantization and further improving the practical value of existing quantization methods.
- For the error vertical accumulation, we design appropriate parameter spaces to employ quantization-aware parameter-efficient fine-tuning, integrating the advantages of post-training quantization and quantization-aware training methods.
- For the error horizontal diffusion, we propose the prompt mixed-precision quantization strategy that ensures the accuracy of important token interactions by retaining a small number of high-precision system prompts cache.
- Extensive experiments on Llama and Qwen families show that BiSup can further improve performance on the top of two state-of-the-art methods (the average WikiText2 perplexity decreases from 13.26 to 9.41 for Atom and from 14.33 to 7.85 for QuaRot under the W3A3-g128 configuration).

2 Related Work

Quantization-Aware Training (QAT) QAT methods (Liu et al., 2023; Dettmers et al., 2024; Li et al., 2023) require substantial data and computational resources to fine-tune the quantized LLMs. To address the challenge of acquiring fine-tuning data, LLM-QAT (Liu et al., 2023) proposes a data-free knowledge distillation method that first utilizes LLMs themselves to generate a large amount of data and then distills the quantized model. To reduce memory consumption during fine-tuning on downstream tasks while addressing the discrepancy between training and inference (i.e., quantization awareness), QLoRA (Dettmers et al., 2024) combines LoRA (Hu et al., 2021) with weight-only quantization, significantly reducing the cost of fine-tuning. Furthermore, LoftQ (Li et al., 2023) indicates the shortcomings of the parameter initialization method used in QLoRA and employs Singular Value Decomposition (SVD) to determine the appropriate low-rank initialization parameters. This initialization technique significantly enhances the generalizability of quantized models.

Post-Training Quantization (PTQ) PTQ methods (Frantar et al., 2022; Shao et al., 2023; Li et al., 2024; Ding et al., 2023) generally require only a small amount of calibration data and computational resources to calibrate the quantized models. One of the most widely used PTQ methods is GPTQ (Frantar et al., 2022), which is compatible with most existing quantization methods and often serves

as an enhanced alternative to the RTN algorithm. GPTQ performs per-channel quantization of all parameters within a block, and after quantizing each channel’s parameters, it appropriately adjusts the remaining unquantized parameters within the block to compensate for the accuracy loss. Recently, given the distinct advantages of QAT and PTQ (where QAT avoids complex algorithm design through gradient optimization and PTQ offers high-yield at low-cost), some studies (Shao et al., 2023; Li et al., 2024; Ding et al., 2023) have explored combining these two approaches which utilize a small amount of data to optimize a carefully designed parameter space. OmniQuant (Shao et al., 2023) and CBQ (Ding et al., 2023) learn appropriate truncation thresholds for weights and smoothing factors for outliers in activations. Norm Tweaking (Li et al., 2024) restricts the trainable parameter space to the weights in the LayerNorm and performs cross-block optimization. Our proposed BiSup makes adaptive improvements based on previous studies by considering weight-activation quantization settings thoroughly.

3 Preliminaries

Quantization techniques involve converting high-precision floating-point numbers into lower-precision representations to reduce the memory and computation requirements of models while maintaining their performance. RTN (round-to-nearest) algorithm is widely utilized due to its simplicity and hardware efficiency, encompassing both asymmetric and symmetric quantization schemas (Nagel et al., 2021). While asymmetric quantization typically offers better performance, symmetric quantization is generally favored in weight-activation quantization settings due to its lower computation and implementation complexities. The quantization process involves two main steps: first calculating the quantization parameters (usually including scale factor and zero point), and then quantizing the input tensor. The quantization parameters (scale factor only since zero point is always equal to 0) for symmetric quantization are determined by (Jacob et al., 2018):

$$\Delta = \frac{\max(|X|)}{2^{N-1} - 1}, \tag{1}$$

where X represents the input tensor to be quantized, N denotes the quantization bit-width, and Δ signifies the scale factor. Subsequently, the input tensor is quantized as follows:

$$\bar{X} = \text{clamp}(\lfloor \frac{X}{\Delta} \rceil, -2^{N-1}, 2^{N-1} - 1), \tag{2}$$

where \bar{X} is the quantized tensor, $\lfloor \cdot \rceil$ denotes the rounding operation, and $\text{clamp}(\cdot)$ represents the truncation operation.

Due to the presence of outliers in the input tensor, applying the same set of quantization parameters to the entire tensor (**tensor-wise**) may lead to degradation, hence quantization is often performed at a finer granularity (**channel/token-wise**), which computing a set of quantization parameters for each row or column in the tensor. Furthermore, each channel/token can be subdivided into multiple groups and quantized within the groups (**group-wise**), which is the most widely used setting in LLMs quantization.

4 Methodology

In this section, we describe the proposed bidirectional quantization error suppression method (BiSup). For the error vertical accumulation, BiSup starts from the weight-activation quantization formula (§4.1), considers the distribution pattern of activation outliers (§4.2) and the convergence of few-shot fine-tuning (§4.3) to design parameter spaces that can be optimized by gradient descent methods (§4.4). For the error horizontal diffusion, by analyzing the distribution of attention weights, we show that LLMs have a strong dependence on the first token. From the perspective of system prompt caching, BiSup introduces the prompt mixed-precision quantization strategy (§4.5) that effectively reduces the error of important token interactions. The overall algorithm is presented in §A.1.

4.1 Fine-Grained Weight-Activation Clipping

Analyzing the equations (1) and (2), it can be seen that although the entire quantization interval contains 2^N integers, the number of actual valid integers is only $2^N - 1$ (where -2^{N-1} is never

taken). When N is small, the resulting bit-width waste is non-negligible. Fortunately, the clipping mechanism adopted in existing methods (Shao et al., 2023; Zhao et al., 2023b; Ashkboos et al., 2024) from the perspective of rounding error can effectively solve this problem, which allows the quantized values to be distributed over the whole interval by truncating the maximum and minimum value. Note that the bit-width waste due to symmetric quantization is also present in activation quantization, so it is necessary to adopt clipping mechanism in both weight and activation quantization, which is often overlooked. The scale factor with the introduction of the clipping mechanism is determined by:

$$\Delta_g = \frac{\max(|X_g|)}{2^{N-1} - 1} \times c, \quad (3)$$

where g is the group index of group-wise quantization and c represents the clip value, which is typically obtained through grid search. However, using the same clip value c for the entire tensor, without considering distribution differences between different groups, leads to sub-optimal results. Therefore, we propose fine-grained weight-activation clipping, where clip values c_g are computed individually for each group and set as a learnable parameter, so that it can be optimized using gradient descent methods along with other parameters instead of grid search. Here, we obtain the optimizable parameter space $\Theta_1 = \{c_g\}$.

4.2 Soft-Constrained Weight-Activation Smoothing

As stated above, it can be observed that activation is more difficult to be quantized due to outliers, while outliers tend to be concentrated in some specific channels. Consequently, some works (Xiao et al., 2023; Shao et al., 2023; Ma et al., 2024) have employed the smoothing mechanism to alleviate this problem, with the core idea being to migrate the difficulty of activation quantization to weight quantization. Specifically, activations are scaled down to smooth the distribution, while weights need to be scaled up to ensure computational invariance. This process can be defined as follows:

$$\langle X \rangle \cdot \langle W \rangle \approx \langle X \text{diag}(s)^{-1} \rangle \cdot \langle \text{diag}(s)W \rangle, \quad (4)$$

where s denotes the smoothing factor, with dimensions equal to the number of columns of X (i.e., the output dimension), and $\langle \cdot \rangle$ represents quantization operation.

To obtain the smoothing factor, SmoothQuant (Xiao et al., 2023) designs an empirical formula, while OmniQuant (Shao et al., 2023) represents it as a learnable parameter. Here, we use the same approach as OmniQuant with improvements. In the original smoothing mechanism, to ensure computational invariance, the transformation matrix applied to activation and weight must satisfy a reversible relationship. However, this constraint is unnecessary in training-based methods since the optimization objective is already able to guarantee invariance. Therefore, we propose soft-constrained weight-activation smoothing to extend flexibility, formalized as:

$$\langle X \rangle \cdot \langle W \rangle \approx \langle X \text{diag}(s_1) \rangle \cdot \langle \text{diag}(s_2)W \rangle, \quad (5)$$

where s_1 and s_2 respectively represent the smoothing factors applied to activation and weight, with the constraint $\text{diag}(s_1) \cdot \text{diag}(s_2) = I$ ensured during parameter initialization. Noting that the optimized s_1 can be integrated into the weight of RMSNorm (Zhang and Sennrich, 2019), and s_2 can be fused into W directly. Thus, the smoothing mechanism incurs no additional overhead during the inference stage. Here, we obtain the optimizable parameter space $\Theta_2 = \{s_1, s_2\}$.

4.3 Stabilized Low-Rank Error Compensation

To compensate quantization errors, ZeroQuant-V2 (Yao et al., 2024) proposes Low-Rank Compensation (LoRC). Given a weight matrix W and quantized counterpart \bar{W} , the weight quantization error $E = W - \bar{W}$. LoRC employs two low-rank matrices \hat{U} and \hat{V} to estimate $\hat{E} = \hat{U}\hat{V}$, where \hat{U} and \hat{V} are obtained by performing Singular Value Decomposition (SVD) on E and selecting the top r singular values. Although LoRC plays well, it requires to retain two additional low-rank matrices and introduces extra computational overhead during inference (i.e., $\hat{Y} = \bar{X}\bar{W} + (\bar{X}\hat{U})\hat{V}$). Furthermore, LoRC falls under the training-free methods, focusing primarily on compensating for weight quantization errors, and struggles to effectively reduce activation quantization errors. Inspired by parameter-efficient fine-tuning methods (Dettmers et al., 2024; Liao and Monz, 2024), we enhance LoRC by making the two low-rank matrices trainable parameters, denoted as A and B , which can be fused into W after optimization. The optimization objective can be formalized as:

$$\underset{A, B}{\operatorname{argmin}} \|XW - \langle X \rangle \langle W + AB \rangle\|_F, \quad (6)$$

where $W \in \mathbb{R}^{d_1 \times d_2}$, $A \in \mathbb{R}^{d_1 \times r}$, $B \in \mathbb{R}^{r \times d_2}$, and r is a fixed hyperparameter. Equation (6) has a similar form to LoRA (Hu et al., 2021) that is widely used. However, as revealed by comparative experiments (§A.3), directly applying it to post-training quantization (usually using a few calibration samples and having a small loss) may be difficult to converge. Therefore, we make an adjustment to Equation (6):

$$\operatorname{argmin}_{A,B} \|XW - \langle X \rangle \langle W \cdot (1 + AB) \rangle\|_F, \quad (7)$$

where W plays the role of anchor to enhance the stability of the optimization. Here, we obtain the optimizable parameter space $\Theta_3 = \{A, B\}$.

4.4 Quantization-Aware Parameter-Efficient Fine-Tuning

In summary, in order to suppress the error vertical accumulation, we construct an optimizable parameter space $\Theta = \{\Theta_1, \Theta_2, \Theta_3\}$. Making a compromise between accuracy and memory consumption, similar with previous work (Shao et al., 2023; Li et al., 2024), we adopt a layer-wise optimization strategy. The optimization objective can be formalized as:

$$\operatorname{argmin}_{\Theta} \|\mathcal{F}(X, W) - \mathcal{F}(\langle \bar{X} \rangle; \Theta_1, \Theta_2), \langle W \rangle; \Theta_1, \Theta_2, \Theta_3)\|_F, \quad (8)$$

where \mathcal{F} denotes a transformer layer, \bar{X} represents the quantized activation produced by the previous layer. Note that we use the quantized activation as the input to the subsequent quantized layer, which enables us to timely eliminate quantization errors. The detailed procedure is shown in Algorithm A1.

4.5 Prompt Mixed-Precision Quantization

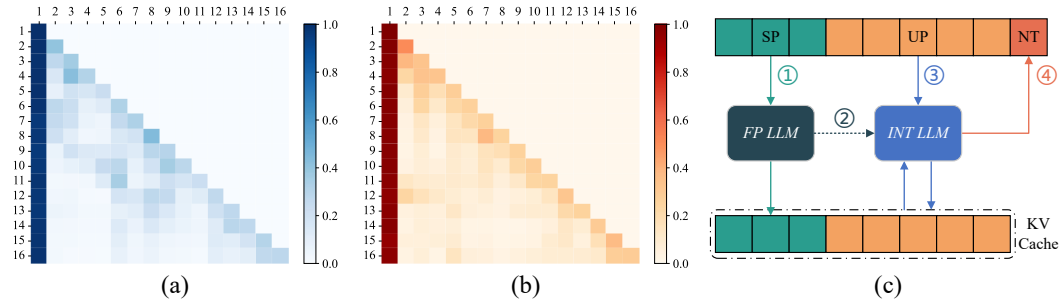


Figure 2: (a) and (b) show the attention maps of Llama3-8B and Llama3-8B-Instruct, respectively, and (c) illustrates the flow of the prompt mixed-precision quantization strategy. The symbols in (c) are explained as follows: SP, UP, and NT represent the system prompt, user prompt, and newly generated next token, respectively. These three elements together constitute the input to the LLM. *FP LLM* refers to the original LLM, while *INT LLM* denotes the quantized counterpart. Step ① indicates encoding and storing the system prompt into the KV cache at high precision. Step ② involves the model quantization. Step ③ describes the inference of the user prompt, which includes interactions with the mixed-precision KV cache. Step ④ denotes the prediction of the next token.

Due to the diffusion of quantization errors through the attention mechanism, it is necessary to analyze the interaction patterns between different tokens within the model. Figure 2 presents the attention maps of Llama3-8B² and Llama3-8B-Instruct³. It can be observed that, regardless of whether undergoing instruction tuning (Zhang et al., 2023), the model exhibits a strong dependency on the first token. Therefore, preserving the accuracy of the first token’s representation contributes to maintaining the interaction patterns among tokens, thereby suppressing error diffusion. More generally, the first token in instruction-tuned LLMs constitutes a part of the system prompt. In system implementation, these fixed special prompts are pre-computed and stored in a key-value cache for reuse across different requests (Kwon et al., 2023). Hence, we propose prompt mixed-precision quantization strategy, effectively reducing errors in the interactions with important tokens by retaining a few system prompt at high precision and quantize the user prompt normally. The detailed process is depicted in Figure 2.

²<https://huggingface.co/meta-llama/Meta-Llama-3-8B>

³<https://huggingface.co/meta-llama/Meta-Llama-3-8B-Instruct>

5 Experiments

We design experiments to address the following research questions (RQs):

- **RQ1:** Can BiSup achieve consistent performance improvements under various quantization configurations, and do all of the proposed techniques work?
- **RQ2:** Does BiSup effectively suppress the error bidirectional propagation?
- **RQ3:** What are the limitations of BiSup and what opportunities exist for its improvement?

To address RQ1, we evaluate the quantized models with language generation tasks and zero-shot tasks under three configurations (§5.2) and conduct ablation studies (§5.3). To tackle RQ2, we compare and analyze the quantization errors of different methods (§5.4). Finally, we discuss the limitations and improvements of BiSup to answer RQ3 (§5.5).

5.1 Settings

Setup We conduct all experiments on RTX 4090 using Hugging Face (Wolf et al., 2020) and PyTorch (Paszke et al., 2019). We apply INT4/INT3 per-channel/token symmetric quantization to weight/activation and per-token asymmetric quantization to key-value cache. Group-wise quantization is represented by ‘g’ (e.g., W4A4-g128 means 4-bit weight/activation quantization with a 128-group size). In our experiments, we always keep the quantization bit-width of the key-value cache consistent with the activation, and the weight and activation have the same group size while the key-value cache is not grouped. Consistent with previous works (Zhao et al., 2023b; Ashkboos et al., 2024), all intermediate activations are quantized except for Q and attention weights. We use grid search to obtain the optimal weight clip value and fix the activation clip value to 0.9 for baselines. We randomly selected 128 samples of length 2048 from WikiText2 (Merity et al., 2016) as the calibration dataset. The r used in stabilized low-rank error compensation is 32. We utilize the AdamW optimizer with a learning rate of 0.005, an epoch of 5, and a batch size of 8. To ensure fairness, we reproduce the baselines to unify all quantification settings and eliminate the effect of package versions on the experimental results.

Models and Tasks We evaluate on Llama (Touvron et al., 2023) and Qwen (Bai et al., 2023) families, which are limited to models up to 32B due to computational constraints. Besides, we also evaluate on the instruction-tuned Llama3-8B-Instruct to verify the generalizability. We report the perplexity of two language generation tasks (including WikiText2 (Merity et al., 2016) and C4 (Raffel et al., 2020)) and the accuracy of six zero-shot tasks (including ARC (Clark et al., 2018), BoolQ (Clark et al., 2019), HellaSwag (Zellers et al., 2019), PIQA (Bisk et al., 2020), and Winogrande (Sakaguchi et al., 2021)).

Baselines Weight-activation quantization primarily involves two directions: mixed precision quantization and outlier suppression. We chose the state-of-the-art (SOTA) approaches from both directions for comparison. Atom (Zhao et al., 2023b) is the SOTA of mixed-precision quantization that retains 128 outlier channels and employs fine-grained per-group quantization (g128). It is notable that in our experiments, Atom is same as QUIK (Ashkboos et al., 2023) when group-wise quantization is not used (i.e., W4A4). QuaRot (Ashkboos et al., 2024) is the SOTA of outlier suppression that introduces offline and online Hadamard transformations to significantly improve outliers in activations at the cost of additional transform overhead. In this paper, Atom_BiSup (or QuaRot_BiSup) denotes using BiSup to suppress quantization errors of the model quantized by Atom (or QuaRot). Note that we do not evaluate QuaRot and QuaRot_BiSup on Qwen family, which would crash due to numerical error accumulation.

5.2 Overall Results

To address RQ1, we evaluate the quantized models using language generation tasks and zero-shot tasks. The partial results of Llama family can be found in Table 1 and Table 2, while the additional results are reported in Appendix (§A.2). As demonstrated in the tables, BiSup consistently achieves performance improvements under the W4A4 and W3A3-g128 configurations, whereas its effect is less significant under W4A4-g128. This indicates that the benefits of BiSup are related to the quantization

Table 1: WikiText2 perplexity results of Llama family. C4 perplexity results of Llama family can be found in Table A1. More perplexity results of Qwen family are in §A.2.

Llama1&2&3 / PPL↓		1-7B	1-13B	1-30B	2-7B	2-13B	3-8B
FP16	-	5.68	5.08	4.09	5.48	4.88	6.14
W4A4	Atom	9.37	8.46	7.44	10.03	8.46	43.60
	Atom_BiSup	7.73	6.98	6.12	7.98	7.11	16.32
	QuaRot	6.27	5.46	4.58	6.16	5.38	8.22
	QuaRot_BiSup	6.01	5.36	4.41	5.88	5.16	7.42
W4A4-g128	Atom	6.15	5.43	4.51	6.02	5.25	7.45
	Atom_BiSup	6.15	5.45	4.53	5.97	5.26	7.55
	QuaRot	6.06	5.40	4.41	5.93	5.25	7.33
	QuaRot_BiSup	5.97	5.31	4.37	5.80	5.11	7.11
W3A3-g128	Atom	10.43	7.99	6.69	12.27	8.68	33.49
	Atom_BiSup	8.45	7.18	6.25	8.76	7.17	18.68
	QuaRot	9.89	7.18	6.26	13.92	8.79	39.95
	QuaRot_BiSup	7.48	6.40	5.48	7.74	6.34	13.69

Table 2: Zero-shot accuracy results of Llama3-8B on Arc-Challenge (A-c), Arc-Easy (A-e), BoolQ (BQ), HellaSwag (HS), PIQA (PQ) and WinoGrande (WG). More results of other models are in §A.2.

Llama3-8B / Acc↑		A-c	A-e	BQ	HS	PQ	WG	Avg.
FP16	-	53.24	80.01	80.98	79.11	80.58	73.01	74.49
W4A4	Atom	26.11	44.70	50.64	42.47	60.12	52.09	46.02
	Atom_BiSup	32.85	63.76	70.37	57.61	69.42	59.83	58.97
	QuaRot	44.45	71.89	74.01	73.09	75.73	66.22	67.57
	QuaRot_BiSup	48.55	78.70	77.43	75.09	77.04	69.46	71.05
W4A4-g128	Atom	48.21	76.89	74.43	75.27	77.42	67.56	69.96
	Atom_BiSup	50.94	79.50	79.72	74.08	78.07	67.25	71.59
	QuaRot	47.78	75.55	79.63	76.17	76.93	71.11	71.20
	QuaRot_BiSup	50.94	79.17	78.96	76.42	78.73	70.96	72.53
W3A3-g128	Atom	24.23	42.05	59.60	42.91	59.03	53.75	46.93
	Atom_BiSup	35.84	64.39	55.69	53.40	68.72	55.96	55.67
	QuaRot	23.81	39.90	56.76	39.95	57.83	51.22	44.91
	QuaRot_BiSup	35.92	67.63	66.79	61.21	71.71	59.91	60.53

difficulty (i.e., the magnitude of quantization error) of different quantization configurations. Under more challenging quantization configurations (namely, W4A4 and W3A3-g128), BiSup can reliably deliver substantial benefits. However, when employing a simpler quantization configuration (i.e., W4A4-g128), BiSup does not show a marked advantage compared to the GPTQ algorithm used in original methods, which quantizes the tensor channel-by-channel and compensates for quantization errors in the unquantized channels. Note that BiSup utilizes the RTN algorithm as an alternative, which is more feasible for fine-tuning. Refer to §5.4 for possible causes of suboptimal performance.

5.3 Ablation Studies

To validate the effectiveness of each technique used in BiSup (RQ2), we conduct ablation experiments starting from the original method (replacing GPTQ with RTN) and progressively incorporating the proposed techniques. As illustrated in Table 3, the four quantization techniques proposed in BiSup are effective across different quantization configurations and original methods. Except for the introduction of the Fine-Grained Weight-Activation Clipping mechanism on Atom (RTN) under W4A4-g128 (7.78 vs. 8.21). To this end, we directly introduce the Soft-Constrained Weight-Activation Smoothing mechanism on the top of Atom (RTN), but obtain similarly poor result (7.84 vs. 7.78). However, when both techniques were applied simultaneously, we achieve better result (7.77 vs. 7.78). Accordingly, we consider this anomaly to be random noise about the hyperparameters. Moreover, the first three proposed techniques have their corresponding original versions. In order to verify the effectiveness of the modifications in this paper, we perform additional comparative experiments in §A.3.

Table 3: Ablation experiment results on different techniques used in BiSup. We report the WikiText2 perplexity of Llama3-8B (serving as a representative model) under three configurations.

Llama-3-8B / PPL↓	W4A4	W4A4-g128	W3A3-g128
Atom (GPTQ)	43.60	7.45	33.49
Atom (RTN)	50.19	7.78	223.76
+ Fine-Grained Weight-Activation Clipping	25.39	8.21	50.29
+ Soft-Constrained Weight-Activation Smoothing	20.03	7.77	34.91
+ Stabilized Low-Rank Error Compensation	17.07	7.57	19.68
+ Prompt Mixed-Precision Quantization	16.32	7.55	18.68
QuaRot (GPTQ)	8.22	7.33	39.95
QuaRot (RTN)	19.08	9.28	4138.60
+ Fine-Grained Weight-Activation Clipping	10.03	8.12	174.81
+ Soft-Constrained Weight-Activation Smoothing	8.13	7.41	21.43
+ Stabilized Low-Rank Error Compensation	7.70	7.22	15.71
+ Prompt Mixed-Precision Quantization	7.42	7.11	13.69

5.4 Error Suppression Analysis

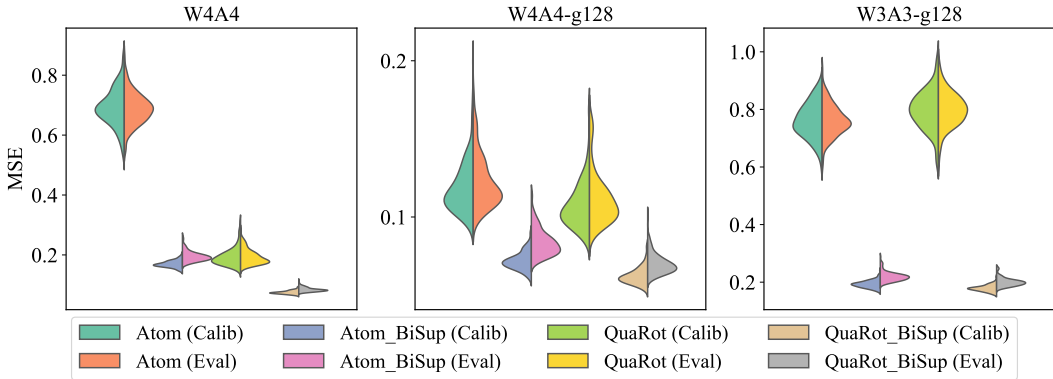


Figure 3: The mean square error (MSE_↓) of the activation of the last decoder layer in Llama3-8B. The dataset used for visualization is WikiText2, where Calib is sampled from the training set (and used to calibrate the quantized model) and Eval is sampled from the test set. Explanation of notation: Atom (Calib) denotes the result of the Atom method on the Calib dataset of WikiText2. Note that due to algorithmic differences, Atom (or Atom_BiSup) and QuaRot (or QuaRot_BiSup) do not have the same activation, so MSE comparisons between these two types of methods make no sense.

To tackle RQ2, we analyze the error propagation of different quantization methods in Llama3-8B. As depicted in Figure 3, the proposed BiSup can learn how to suppress error propagation on the calibration dataset and effectively generalize to other datasets. Corresponding to §5.2, it can be observed that under W4A4 and W3A3-g128, BiSup significantly suppresses the quantization errors (the error suppression rate is about 70% in the last layer). In contrast, under W4A4-g128, the error suppression rate is only about 30%. One reason is that under W4A4-g128, the errors introduced by the quantized model are rather small, making it more difficult to optimize. Furthermore, we observe an inconsistency between quantization errors and final results: while in most cases smaller quantization errors typically correspond to lower perplexity, we note that under W4A4-g128, Atom_BiSup (Eval) exhibits smaller quantization errors compared to Atom (Eval), but Atom (Eval) demonstrates lower perplexity (7.45 vs. 7.55 in Table 1). This finding indicates a difference between the currently widely used layer-wise optimization strategy based on mean square error and the overall optimization strategy based on cross-entropy loss of the final results. The layer-wise optimization strategy can effectively indicate the direction of optimization under challenging quantization configurations. However, when under simpler quantization configurations, it tends to fall into local optima. This finding reveals a potential reason for the suboptimal performance of BiSup under W4A4-g128. Besides, it is well

known that the performance of gradient-based algorithms is related to the hyperparameters. Thus, we conduct experiments on the core hyperparameters of BiSup in §A.4 for further discussion.

5.5 Limitations and Improvements

In summary, BiSup is capable of improving performance under different settings, but it also shows some limitations and opportunities for improvement (RQ3).

Improvements of Layer-wise Optimization Strategy As analyzed in §5.4, the layer-wise optimization strategy, which does not adequately correlate with the final results, can lead to local optima. As an alternative, cross-layer optimization strategies that optimize multiple layers simultaneously could be considered. Additionally, different elements in the weights and activations have different importance (e.g. outliers are particularly important), which could be taken into account when designing the loss function (e.g., by introducing the weighted mean square error).

Best Practices for Quantization-Aware Parameter-Efficient Fine-Tuning As shown in the hyperparameter studies (§A.4), fine-tuning with more samples and iterations can yield better results. However, quantization techniques require a trade-off between memory consumption, time cost, and final performance. To this end, exploring the use of a small amount of high-quality data instead of large volumes of low-quality data, and investigating parameter initialization methods that align more closely with the quantization settings for faster convergence, could be beneficial.

Adequate Exploration of Prompt Mixed-Precision Quantization As indicated by the ablation studies (§5.3), while the prompt mixed-precision quantization strategy is effective, it has a limited impact on error suppression, with most of the contribution coming from fine-tuning. This is partly because the system prompts involved in our experiments are very short (e.g., non-instruction tuned models include only a single <bos> token). Experiments on more complex real-world scenarios are needed. Furthermore, the proposed prompt mixed-precision quantization strategy mainly focuses on system prompts. In practice, important tokens also exist in user prompts, which can be dynamically identified and preserved at high precision during inference (Yang et al., 2024).

6 Conclusion

Existing weight-activation quantization methods highlight optimizing the results of single matrix multiplication, overlooking the bidirectional propagation of quantization errors within the model, which includes the vertical accumulation within the same token and the horizontal diffusion across different tokens. To mitigate error propagation, We propose BiSup that constructs appropriate parameter spaces and applies quantization-aware parameter-efficient fine-tuning to compensate for quantization error in a timely manner, incorporating prompt mixed-precision quantization for the protection of important token interaction patterns. Extensive experiments on Llama and Qwen families validate the effectiveness of BiSup, and we conclude with a discussion of the limitations and improvements of BiSup.

References

- Saleh Ashkboos, Iliia Markov, Elias Frantar, Tingxuan Zhong, Xincheng Wang, Jie Ren, Torsten Hoefler, and Dan Alistarh. 2023. Quik: Towards end-to-end 4-bit inference on generative large language models. *arXiv preprint arXiv:2310.09259*.
- Saleh Ashkboos, Amirkeivan Mohtashami, Maximilian L Croci, Bo Li, Martin Jaggi, Dan Alistarh, Torsten Hoefler, and James Hensman. 2024. Quarot: Outlier-free 4-bit inference in rotated llms. *arXiv preprint arXiv:2404.00456*.
- Jinze Bai, Shuai Bai, Yunfei Chu, Zeyu Cui, Kai Dang, Xiaodong Deng, Yang Fan, Wenbin Ge, Yu Han, Fei Huang, Binyuan Hui, Luo Ji, Mei Li, Junyang Lin, Runji Lin, Dayiheng Liu, Gao Liu, Chengqiang Lu, Keming Lu, Jianxin Ma, Rui Men, Xingzhang Ren, Xuancheng Ren, Chuanqi Tan, Sinan Tan, Jianhong Tu, Peng Wang, Shijie Wang, Wei Wang, Shengguang Wu, Benfeng Xu, Jin Xu, An Yang, Hao Yang, Jian Yang, Shusheng Yang, Yang Yao, Bowen Yu, Hongyi Yuan, Zheng Yuan, Jianwei Zhang, Xingxuan Zhang, Yichang Zhang, Zhenru Zhang, Chang Zhou, Jingren Zhou, Xiaohuan Zhou, and Tianhang Zhu. 2023. Qwen technical report. *arXiv preprint arXiv:2309.16609*.
- Yonatan Bisk, Rowan Zellers, Jianfeng Gao, Yejin Choi, et al. 2020. Piqa: Reasoning about physical commonsense in natural language. In *Proceedings of the AAAI conference on artificial intelligence*, volume 34, pages 7432–7439.
- Christopher Clark, Kenton Lee, Ming-Wei Chang, Tom Kwiatkowski, Michael Collins, and Kristina Toutanova. 2019. Boolq: Exploring the surprising difficulty of natural yes/no questions. *arXiv preprint arXiv:1905.10044*.
- Peter Clark, Isaac Cowhey, Oren Etzioni, Tushar Khot, Ashish Sabharwal, Carissa Schoenick, and Oyvind Tafjord. 2018. Think you have solved question answering? try arc, the ai2 reasoning challenge. *arXiv preprint arXiv:1803.05457*.
- Tim Dettmers, Mike Lewis, Younes Belkada, and Luke Zettlemoyer. 2022. Gpt3. int8 (): 8-bit matrix multiplication for transformers at scale. *Advances in Neural Information Processing Systems*, 35:30318–30332.
- Tim Dettmers, Artidoro Pagnoni, Ari Holtzman, and Luke Zettlemoyer. 2024. Qlora: Efficient finetuning of quantized llms. *Advances in Neural Information Processing Systems*, 36.
- Xin Ding, Xiaoyu Liu, Yun Zhang, Zhijun Tu, Wei Li, Jie Hu, Hanting Chen, Yehui Tang, Zhiwei Xiong, Baoqun Yin, et al. 2023. Cbq: Cross-block quantization for large language models. *arXiv preprint arXiv:2312.07950*.
- Elias Frantar, Saleh Ashkboos, Torsten Hoefler, and Dan Alistarh. 2022. Optq: Accurate quantization for generative pre-trained transformers. In *The Eleventh International Conference on Learning Representations*.
- Cong Guo, Jiaming Tang, Weiming Hu, Jingwen Leng, Chen Zhang, Fan Yang, Yunxin Liu, Minyi Guo, and Yuhao Zhu. 2023. Olive: Accelerating large language models via hardware-friendly outlier-victim pair quantization. In *Proceedings of the 50th Annual International Symposium on Computer Architecture*, pages 1–15.
- Edward J Hu, Yelong Shen, Phillip Wallis, Zeyuan Allen-Zhu, Yuanzhi Li, Shean Wang, Lu Wang, and Weizhu Chen. 2021. Lora: Low-rank adaptation of large language models. *arXiv preprint arXiv:2106.09685*.
- Benoit Jacob, Skirmantas Kligys, Bo Chen, Menglong Zhu, Matthew Tang, Andrew Howard, Hartwig Adam, and Dmitry Kalenichenko. 2018. Quantization and training of neural networks for efficient integer-arithmetic-only inference. In *Proceedings of the IEEE conference on computer vision and pattern recognition*, pages 2704–2713.
- Woosuk Kwon, Zhuohan Li, Siyuan Zhuang, Ying Sheng, Lianmin Zheng, Cody Hao Yu, Joseph Gonzalez, Hao Zhang, and Ion Stoica. 2023. Efficient memory management for large language model serving with pagedattention. In *Proceedings of the 29th Symposium on Operating Systems Principles*, pages 611–626.

- Liang Li, Qingyuan Li, Bo Zhang, and Xiangxiang Chu. 2024. Norm tweaking: High-performance low-bit quantization of large language models. In *Proceedings of the AAAI Conference on Artificial Intelligence*, volume 38, pages 18536–18544.
- Yixiao Li, Yifan Yu, Chen Liang, Pengcheng He, Nikos Karampatziakis, Weizhu Chen, and Tuo Zhao. 2023. Loftq: Lora-fine-tuning-aware quantization for large language models. *arXiv preprint arXiv:2310.08659*.
- Baohao Liao and Christof Monz. 2024. Apiq: Finetuning of 2-bit quantized large language model. *arXiv preprint arXiv:2402.05147*.
- Ji Lin, Jiaming Tang, Haotian Tang, Shang Yang, Xingyu Dang, and Song Han. 2023. Awq: Activation-aware weight quantization for llm compression and acceleration. *arXiv preprint arXiv:2306.00978*.
- Zechun Liu, Barlas Oguz, Changsheng Zhao, Ernie Chang, Pierre Stock, Yashar Mehdad, Yangyang Shi, Raghuraman Krishnamoorthi, and Vikas Chandra. 2023. Llm-qat: Data-free quantization aware training for large language models. *arXiv preprint arXiv:2305.17888*.
- Yuexiao Ma, Huixia Li, Xiawu Zheng, Feng Ling, Xuefeng Xiao, Rui Wang, Shilei Wen, Fei Chao, and Rongrong Ji. 2024. Affinequant: Affine transformation quantization for large language models. *arXiv preprint arXiv:2403.12544*.
- Stephen Merity, Caiming Xiong, James Bradbury, and Richard Socher. 2016. Pointer sentinel mixture models. *arXiv preprint arXiv:1609.07843*.
- Markus Nagel, Marios Fournarakis, Rana Ali Amjad, Yelysei Bondarenko, Mart Van Baalen, and Tijmen Blankevoort. 2021. A white paper on neural network quantization. *arXiv preprint arXiv:2106.08295*.
- Adam Paszke, Sam Gross, Francisco Massa, Adam Lerer, James Bradbury, Gregory Chanan, Trevor Killeen, Zeming Lin, Natalia Gimelshein, Luca Antiga, et al. 2019. Pytorch: An imperative style, high-performance deep learning library. *Advances in neural information processing systems*, 32.
- Colin Raffel, Noam Shazeer, Adam Roberts, Katherine Lee, Sharan Narang, Michael Matena, Yanqi Zhou, Wei Li, and Peter J Liu. 2020. Exploring the limits of transfer learning with a unified text-to-text transformer. *Journal of machine learning research*, 21:1–67.
- Keisuke Sakaguchi, Ronan Le Bras, Chandra Bhagavatula, and Yejin Choi. 2021. Winogrande: An adversarial winograd schema challenge at scale. *Communications of the ACM*, 64(9):99–106.
- Wenqi Shao, Mengzhao Chen, Zhaoyang Zhang, Peng Xu, Lirui Zhao, Zhiqian Li, Kaipeng Zhang, Peng Gao, Yu Qiao, and Ping Luo. 2023. Omniquant: Omnidirectionally calibrated quantization for large language models. *arXiv preprint arXiv:2308.13137*.
- Hugo Touvron, Thibaut Lavril, Gautier Izacard, Xavier Martinet, Marie-Anne Lachaux, Timothée Lacroix, Baptiste Rozière, Naman Goyal, Eric Hambro, Faisal Azhar, Aurelien Rodriguez, Armand Joulin, Edouard Grave, and Guillaume Lample. 2023. Llama: Open and efficient foundation language models. *arXiv preprint arXiv:2302.13971*.
- Wenxiao Wang, Wei Chen, Yicong Luo, Yongliu Long, Zhengkai Lin, Liye Zhang, Binbin Lin, Deng Cai, and Xiaofei He. 2024. Model compression and efficient inference for large language models: A survey. *arXiv preprint arXiv:2402.09748*.
- Thomas Wolf, Lysandre Debut, Victor Sanh, Julien Chaumond, Clement Delangue, Anthony Moi, Pierric Cistac, Tim Rault, Rémi Louf, Morgan Funtowicz, et al. 2020. Transformers: State-of-the-art natural language processing. In *Proceedings of the 2020 conference on empirical methods in natural language processing: system demonstrations*, pages 38–45.
- Guangxuan Xiao, Ji Lin, Mickael Seznec, Hao Wu, Julien Demouth, and Song Han. 2023. Smoothquant: Accurate and efficient post-training quantization for large language models. In *International Conference on Machine Learning*, pages 38087–38099. PMLR.
- June Yong Yang, Byeongwook Kim, Jeongin Bae, Beomseok Kwon, Gunho Park, Eunho Yang, Se Jung Kwon, and Dongsoo Lee. 2024. No token left behind: Reliable kv cache compression via importance-aware mixed precision quantization. *arXiv preprint arXiv:2402.18096*.

- Zhewei Yao, Xiaoxia Wu, Cheng Li, Stephen Youn, and Yuxiong He. 2024. Exploring post-training quantization in llms from comprehensive study to low rank compensation. In *Proceedings of the AAAI Conference on Artificial Intelligence*, volume 38, pages 19377–19385.
- Rowan Zellers, Ari Holtzman, Yonatan Bisk, Ali Farhadi, and Yejin Choi. 2019. Hellaswag: Can a machine really finish your sentence? *arXiv preprint arXiv:1905.07830*.
- Biao Zhang and Rico Sennrich. 2019. Root mean square layer normalization. *Advances in Neural Information Processing Systems*, 32.
- Shengyu Zhang, Linfeng Dong, Xiaoya Li, Sen Zhang, Xiaofei Sun, Shuhe Wang, Jiwei Li, Runyi Hu, Tianwei Zhang, Fei Wu, et al. 2023. Instruction tuning for large language models: A survey. *arXiv preprint arXiv:2308.10792*.
- Wayne Xin Zhao, Kun Zhou, Junyi Li, Tianyi Tang, Xiaolei Wang, Yupeng Hou, Yingqian Min, Beichen Zhang, Junjie Zhang, Zican Dong, et al. 2023a. A survey of large language models. *arXiv preprint arXiv:2303.18223*.
- Yilong Zhao, Chien-Yu Lin, Kan Zhu, Zihao Ye, Lequn Chen, Size Zheng, Luis Ceze, Arvind Krishnamurthy, Tianqi Chen, and Baris Kasikci. 2023b. Atom: Low-bit quantization for efficient and accurate llm serving. *arXiv preprint arXiv:2310.19102*.
- Xunyu Zhu, Jian Li, Yong Liu, Can Ma, and Weiping Wang. 2023. A survey on model compression for large language models. *arXiv preprint arXiv:2308.07633*.

A Appendix

In this appendix, we provide more details as follows:

- §A.1: Pseudo-code for our BiSup algorithm.
- §A.2: Additional overall results for Llama and Qwen families.
- §A.3: Comparative experiments between the proposed techniques and their original versions.
- §A.4: Hyperparameter studies in quantization-aware parameter-efficient fine-tuning.

A.1 Overall Algorithm

The workflow of our BiSup is demonstrated in Algorithm A1, which consists of four main steps: preprocessing the model according to the needs of Atom or QuaRot (Line 1), calculating and storing high-precision system prompts (Line 2), initializing learnable parameters and performing gradient optimization (Lines 3-16), and finally quantizing the model (Line 17).

Algorithm A1 Overall Algorithm of BiSup

Input: calibration dataset X , LLM \mathcal{M} , hadamard matrix H

Output: quantized $\hat{\mathcal{M}}$

```
1: reorder (or rotate)  $\mathcal{M}$  using  $X$  (or  $H$ )                                ▷ preprocessing of Atom (or QuaRot)
2: calculate full-precision kv cache of system prompts with  $\mathcal{M}$           ▷ §4.5
3:  $X_{fp} = X_{int} = X$                                                     ▷ init the inputs of the transformer layers
4: for  $\mathcal{L}_i$  in  $\mathcal{M}$  do                                                    ▷ layer-wise optimization
5:   convert  $\mathcal{L}_i$  from FP16 to BF16                                       ▷ prevent numerical overflow
6:    $X_{fp} = \mathcal{L}_i(X_{fp})$                                                ▷ update full-precision inputs
7:   init learnable parameters  $\Theta = \{\Theta_1, \Theta_2, \Theta_3\}$       ▷ §4.1, §4.2, and §4.3
8:   for e in epochs do
9:     for  $(x_{fp}, x_{int})$  in  $(X_{fp}, X_{int})$  do                          ▷ §4.4
10:       $x_{int} = \mathcal{L}_i(x_{int}; \Theta)$                                   ▷ quantize and forward
11:      loss =  $\|x_{int} - x_{fp}\|^2$                                           ▷ MSELoss
12:      backward and update  $\Theta$  through gradient                          ▷ with AdamW optimizer
13:    end for
14:  end for
15:   $X_{int} = \mathcal{L}_i(X_{int}; \Theta)$                                        ▷ update quantized inputs
16:  revert  $\mathcal{L}_i$  from BF16 to FP16                                         ▷ revert the data type
17:   $\hat{\mathcal{L}}_i$  in  $\hat{\mathcal{M}} \leftarrow \text{Quantize}(\mathcal{L}_i, \Theta)$           ▷ quantize the transformer layer
18: end for
```

A.2 Additional Overall Results

In this section, we provide additional overall results for Llama and Qwen families. The list of tables is as follows:

- Table A1: C4 perplexity results of Llama family.
- Table A2: Zero-shot accuracy results of Llama family under W4A4.
- Table A3: Zero-shot accuracy results of Llama family under W4A4-g128.
- Table A4: Zero-shot accuracy results of Llama family under W3A3-g128.
- Table A5: Zero-shot accuracy results of Llama3-8B-Instruct.
- Table A6: WikiText2 perplexity results of Qwen family.
- Table A7: C4 perplexity results of Qwen family.
- Table A8: Zero-shot accuracy results of Qwen family under W4A4.
- Table A9: Zero-shot accuracy results of Qwen family under W4A4-g128.
- Table A10: Zero-shot accuracy results of Qwen family under W3A3-g128.

Table A1: C4 perplexity results of Llama family.

Llama1&2&3 / PPL↓		1-7B	1-13B	1-30B	2-7B	2-13B	3-8B
FP16	-	7.08	6.60	5.98	6.97	6.46	8.88
W4A4	Atom	11.97	11.02	9.83	13.07	11.12	58.34
	Atom_BiSup	10.23	9.31	8.46	10.76	9.77	22.30
	QuaRot	7.81	7.06	6.37	7.80	7.07	11.87
	QuaRot_BiSup	7.55	6.94	6.27	7.57	6.84	10.88
W4A4-g128	Atom	7.67	7.00	6.33	7.68	6.92	10.90
	Atom_BiSup	7.74	7.09	6.40	7.70	7.02	11.16
	QuaRot	7.59	6.92	6.24	7.54	6.91	10.68
	QuaRot_BiSup	7.48	6.89	6.23	7.43	6.78	10.40
W3A3-g128	Atom	13.32	10.31	8.83	15.57	11.53	50.05
	Atom_BiSup	11.25	9.68	8.56	11.92	9.95	25.94
	QuaRot	12.58	9.27	8.44	18.70	12.09	50.90
	QuaRot_BiSup	9.70	8.41	7.47	10.46	8.57	19.60

Table A2: Zero-shot accuracy results of Llama family under W4A4.

Llama1&2 / Acc↑		A-c	A-e	BQ	HS	PQ	WG	Avg.
1-7B	FP16	44.20	75.46	76.79	76.05	79.27	70.24	70.33
	Atom	37.20	62.29	65.29	63.94	70.13	58.56	59.57
	Atom_BiSup	34.98	66.92	66.70	64.11	73.34	62.35	61.40
	QuaRot	40.10	72.26	75.38	72.87	76.88	67.48	67.50
	QuaRot_BiSup	42.15	74.20	75.75	72.85	77.97	68.43	68.56
1-13B	FP16	48.38	77.31	79.85	79.30	79.98	73.40	73.04
	Atom	36.35	62.42	65.38	69.30	72.31	61.33	61.18
	Atom_BiSup	39.08	71.25	67.19	68.79	74.54	64.96	64.30
	QuaRot	46.25	75.46	77.31	76.84	78.89	70.56	70.89
	QuaRot_BiSup	46.42	76.18	78.26	77.19	79.92	71.98	71.66
1-30B	FP16	53.58	80.64	83.82	83.01	81.83	75.93	76.47
	Atom	38.91	62.46	71.99	70.77	71.93	60.62	62.78
	Atom_BiSup	42.15	75.08	76.57	73.16	76.55	68.82	68.72
	QuaRot	51.11	78.70	82.84	80.82	80.52	74.74	74.79
	QuaRot_BiSup	52.05	79.92	81.47	81.05	80.41	75.77	75.11
2-7B	FP16	45.05	75.51	79.33	76.17	78.84	69.38	70.71
	Atom	36.18	58.38	63.88	61.39	67.63	58.25	57.62
	Atom_BiSup	34.90	66.67	65.57	63.90	72.74	62.04	60.97
	QuaRot	41.47	72.39	74.31	72.17	76.77	65.82	67.16
	QuaRot_BiSup	43.86	74.71	75.44	72.71	77.75	66.30	68.46
2-13B	FP16	48.72	78.96	82.14	79.63	80.36	72.53	73.72
	Atom	36.77	63.05	65.41	66.00	71.00	58.96	60.20
	Atom_BiSup	38.14	70.83	69.42	67.64	74.92	64.80	64.29
	QuaRot	46.42	76.30	78.78	76.18	78.45	71.35	71.25
	QuaRot_BiSup	47.10	78.07	81.41	77.38	79.38	71.98	72.55

Table A3: Zero-shot accuracy results of Llama family under W4A4-g128.

Llama1&2 / Acc \uparrow	A-c	A-e	BQ	HS	PQ	WG	Avg.	
1-7B	FP16	44.20	75.46	76.79	76.05	79.27	70.24	70.33
	Atom	40.87	72.60	74.13	72.66	76.66	66.93	67.31
	Atom_BiSup	41.21	72.98	73.39	72.17	76.61	66.61	67.16
	QuaRot	43.34	72.98	75.50	73.16	77.86	68.82	68.61
	QuaRot_BiSup	41.55	73.74	74.62	73.53	78.07	68.27	68.30
1-13B	FP16	48.38	77.31	79.85	79.30	79.98	73.40	73.04
	Atom	45.31	75.25	77.43	77.12	78.02	70.09	70.54
	Atom_BiSup	45.48	76.85	77.28	75.81	78.73	70.96	70.85
	QuaRot	45.39	75.17	78.50	77.05	79.27	71.90	71.21
	QuaRot_BiSup	45.90	75.80	78.47	77.25	79.92	72.06	71.57
1-30B	FP16	53.58	80.64	83.82	83.01	81.83	75.93	76.47
	Atom	50.26	78.96	82.29	80.77	80.30	74.74	74.55
	Atom_BiSup	50.85	79.63	82.05	80.00	80.69	75.06	74.71
	QuaRot	52.39	79.38	81.44	81.29	80.74	75.06	75.05
	QuaRot_BiSup	52.56	79.76	83.00	80.98	80.79	74.59	75.28
2-7B	FP16	45.05	75.51	79.33	76.17	78.84	69.38	70.71
	Atom	41.72	72.39	73.94	72.94	77.42	65.51	67.32
	Atom_BiSup	42.06	73.53	74.65	72.44	76.93	68.82	68.07
	QuaRot	45.05	73.48	74.16	73.55	78.40	65.11	68.29
	QuaRot_BiSup	42.66	73.86	76.24	73.23	78.29	66.30	68.43
2-13B	FP16	48.72	78.96	82.14	79.63	80.36	72.53	73.72
	Atom	46.42	76.30	80.80	77.21	78.89	69.61	71.54
	Atom_BiSup	45.90	77.15	78.53	76.38	78.51	71.35	71.30
	QuaRot	47.18	77.53	81.07	77.74	79.60	71.43	72.42
	QuaRot_BiSup	48.12	77.90	81.28	77.57	79.60	71.59	72.68

Table A4: Zero-shot accuracy results of Llama family under W3A3-g128.

Llama1&2 / Acc \uparrow	A-c	A-e	BQ	HS	PQ	WG	Avg.	
1-7B	FP16	44.20	75.46	76.79	76.05	79.27	70.24	70.33
	Atom	29.69	59.22	63.85	56.40	68.12	56.04	55.55
	Atom_BiSup	33.62	64.98	66.18	59.44	70.78	60.38	59.23
	QuaRot	31.40	59.64	64.13	56.91	68.66	56.12	56.14
	QuaRot_BiSup	36.18	68.60	69.48	64.71	74.16	60.14	62.21
1-13B	FP16	48.38	77.31	79.85	79.30	79.98	73.40	73.04
	Atom	34.98	63.26	66.97	64.88	72.25	59.19	60.25
	Atom_BiSup	36.77	69.87	69.11	65.61	73.83	63.38	63.09
	QuaRot	37.97	68.94	68.81	67.95	74.21	63.14	63.50
	QuaRot_BiSup	41.47	72.14	73.36	70.95	77.04	68.27	67.20
1-30B	FP16	53.58	80.64	83.82	83.01	81.83	75.93	76.47
	Atom	42.06	69.36	72.84	70.94	74.48	66.30	66.00
	Atom_BiSup	41.64	73.78	71.74	71.71	75.35	68.75	67.16
	QuaRot	41.38	71.00	74.68	71.40	75.57	66.30	66.72
	QuaRot_BiSup	46.76	76.30	78.96	75.57	78.40	70.88	71.14
2-7B	FP16	45.05	75.51	79.33	76.17	78.84	69.38	70.71
	Atom	28.41	53.66	59.20	49.80	63.17	53.59	51.31
	Atom_BiSup	34.81	64.56	68.04	58.90	70.24	58.33	59.15
	QuaRot	30.72	56.94	60.12	47.76	65.61	54.62	52.63
	QuaRot_BiSup	33.96	65.95	66.73	63.06	72.80	61.09	60.60
2-13B	FP16	48.72	78.96	82.14	79.63	80.36	72.53	73.72
	Atom	33.45	64.48	69.20	60.12	70.24	58.96	59.41
	Atom_BiSup	38.91	70.08	71.25	65.69	74.59	66.06	64.43
	QuaRot	32.76	60.06	66.09	58.40	67.46	53.99	56.46
	QuaRot_BiSup	41.38	73.99	78.38	70.86	75.08	66.69	67.73

Table A5: Zero-shot accuracy results of Llama3-8B-Instruct.

Llama3-8B-Instruct / Acc \uparrow		A-c	A-e	BQ	HS	PQ	WG	Avg.
FP16	-	57.08	81.52	83.27	75.80	79.00	72.45	74.85
W4A4	Atom	28.84	47.85	52.75	46.52	61.15	53.99	48.52
	Atom_BiSup	36.35	66.62	76.12	56.25	67.19	60.38	60.48
	QuaRot	46.25	75.93	79.85	70.98	75.57	66.77	69.22
	QuaRot_BiSup	50.68	79.17	82.72	72.18	76.39	68.67	71.64
W4A4-g128	Atom	50.17	77.31	80.49	72.78	76.01	70.32	71.18
	Atom_BiSup	51.79	79.76	82.48	71.44	76.12	68.11	71.62
	QuaRot	50.09	78.28	81.62	73.23	75.63	67.72	71.10
	QuaRot_BiSup	51.71	80.56	82.54	72.99	76.71	69.30	72.30
W3A3-g128	Atom	28.33	48.95	56.91	43.71	60.28	52.88	48.51
	Atom_BiSup	36.69	66.88	65.57	54.22	69.15	57.46	58.33
	QuaRot	24.32	41.12	53.03	41.86	58.54	52.41	45.21
	QuaRot_BiSup	40.78	70.54	74.19	58.75	71.71	60.62	62.76

Table A6: WikiText2 perplexity results of Qwen family.

Qwen1.5 / PPL \downarrow		0.5B	1.8B	4B	7B	14B	32B
FP16	-	14.81	11.45	8.94	7.95	7.45	6.17
W4A4	Atom	34.47	20.20	15.04	14.69	14.67	16.65
	Atom_BiSup	21.75	15.76	14.21	11.92	10.17	8.65
W4A4-g128	Atom	22.40	13.31	10.00	8.72	7.95	6.58
	Atom_BiSup	18.07	12.99	10.69	8.97	7.98	6.57
W3A3-g128	Atom	267.08	40.50	21.41	14.64	10.76	9.55
	Atom_BiSup	32.94	21.47	17.33	14.09	10.51	8.45

Table A7: C4 perplexity results of Qwen family.

Qwen1.5 / PPL \downarrow		0.5B	1.8B	4B	7B	14B	32B
FP16	-	17.38	13.96	12.12	11.01	10.22	8.34
W4A4	Atom	43.99	25.01	20.20	20.06	20.83	23.08
	Atom_BiSup	30.97	21.58	20.06	17.31	14.77	12.46
W4A4-g128	Atom	26.68	16.45	13.62	12.15	10.95	8.94
	Atom_BiSup	23.40	16.52	14.81	12.49	11.23	9.09
W3A3-g128	Atom	284.60	46.86	27.98	20.37	14.87	12.97
	Atom_BiSup	53.22	31.72	26.06	20.98	15.60	12.70

Table A8: Zero-shot accuracy results of Qwen family under W4A4.

Qwen1.5 / Acc \uparrow		A-c	A-e	BQ	HS	PQ	WG	Avg.
0.5B	FP16	29.18	57.11	49.66	49.28	69.48	55.25	51.66
	Atom	24.91	42.85	52.39	36.10	59.90	48.62	44.13
	Atom_BiSup	26.54	47.73	61.68	38.89	62.30	51.62	48.13
1.8B	FP16	34.56	64.77	66.39	60.88	74.43	61.48	60.42
	Atom	28.41	52.90	62.26	49.18	65.40	54.14	52.05
	Atom_BiSup	29.61	54.88	62.72	48.70	66.43	56.35	53.12
4B	FP16	39.68	68.22	77.77	71.42	77.04	63.77	66.32
	Atom	31.57	57.91	59.63	58.39	68.01	55.88	55.23
	Atom_BiSup	29.44	51.47	65.05	52.61	63.11	52.64	52.39
7B	FP16	42.92	71.00	82.39	76.89	79.33	65.90	69.74
	Atom	32.25	59.72	59.79	62.88	69.70	55.33	56.61
	Atom_BiSup	36.01	68.06	70.18	61.94	71.11	58.01	60.88
14B	FP16	47.10	74.54	85.54	79.44	79.65	71.03	72.88
	Atom	39.33	61.99	67.95	66.89	70.67	57.93	60.79
	Atom_BiSup	42.83	72.18	79.66	69.23	75.03	64.88	67.30
32B	FP16	50.94	77.53	87.37	83.73	82.59	74.19	76.06
	Atom	35.58	54.25	51.07	64.16	67.41	55.49	54.66
	Atom_BiSup	47.27	75.67	81.90	73.66	78.67	71.43	71.43

Table A9: Zero-shot accuracy results of Qwen family under W4A4-g128.

Qwen1.5 / Acc \uparrow	A-c	A-e	BQ	HS	PQ	WG	Avg.	
0.5B	FP16	29.18	57.11	49.66	49.28	69.48	55.25	51.66
	Atom	27.39	49.92	54.98	42.01	64.15	50.99	48.24
	Atom_BiSup	27.30	49.20	60.40	42.69	64.74	53.43	49.63
1.8B	FP16	34.56	64.77	66.39	60.88	74.43	61.48	60.42
	Atom	32.51	61.49	64.68	56.35	71.11	57.06	57.20
	Atom_BiSup	31.31	61.91	65.20	54.64	71.27	58.56	57.15
4B	FP16	39.68	68.22	77.77	71.42	77.04	63.77	66.32
	Atom	37.29	63.89	72.51	67.38	74.37	59.98	62.57
	Atom_BiSup	33.96	60.56	72.05	61.59	68.88	59.12	59.36
7B	FP16	42.92	71.00	82.39	76.89	79.33	65.90	69.74
	Atom	41.72	69.02	76.36	73.66	76.77	64.33	66.98
	Atom_BiSup	43.69	71.93	80.43	72.32	77.42	64.40	68.37
14B	FP16	47.10	74.54	85.54	79.44	79.65	71.03	72.88
	Atom	45.31	73.82	83.61	77.80	79.00	68.35	71.31
	Atom_BiSup	47.10	75.46	84.62	76.49	78.73	70.24	72.11
32B	FP16	50.94	77.53	87.37	83.73	82.59	74.19	76.06
	Atom	51.37	77.23	86.06	81.96	82.05	73.56	75.37
	Atom_BiSup	50.26	77.36	86.39	80.60	81.61	74.82	75.17

Table A10: Zero-shot accuracy results of Qwen family under W3A3-g128.

Qwen1.5 / Acc \uparrow	A-c	A-e	BQ	HS	PQ	WG	Avg.	
0.5B	FP16	29.18	57.11	49.66	49.28	69.48	55.25	51.66
	Atom	24.91	30.01	50.21	27.29	52.39	50.36	39.20
	Atom_BiSup	22.35	41.04	61.28	32.56	58.16	49.96	44.23
1.8B	FP16	34.56	64.77	66.39	60.88	74.43	61.48	60.42
	Atom	25.09	43.35	58.35	39.45	60.50	53.20	46.66
	Atom_BiSup	24.23	48.61	62.11	40.99	63.71	52.33	48.66
4B	FP16	39.68	68.22	77.77	71.42	77.04	63.77	66.32
	Atom	29.86	50.29	58.32	49.04	64.80	55.09	51.23
	Atom_BiSup	27.13	49.20	63.88	45.30	61.10	52.49	49.85
7B	FP16	42.92	71.00	82.39	76.89	79.33	65.90	69.74
	Atom	33.19	58.04	63.43	57.95	67.52	55.96	56.01
	Atom_BiSup	33.45	64.48	66.24	55.86	69.37	61.80	58.53
14B	FP16	47.10	74.54	85.54	79.44	79.65	71.03	72.88
	Atom	41.55	65.74	70.28	69.38	72.85	62.04	63.64
	Atom_BiSup	42.32	71.17	76.73	65.94	74.27	64.96	65.90
32B	FP16	50.94	77.53	87.37	83.73	82.59	74.19	76.06
	Atom	42.06	70.58	74.56	71.57	77.48	63.22	66.58
	Atom_BiSup	46.25	75.21	78.72	70.92	77.09	70.80	69.83

A.3 Comparative Experiments

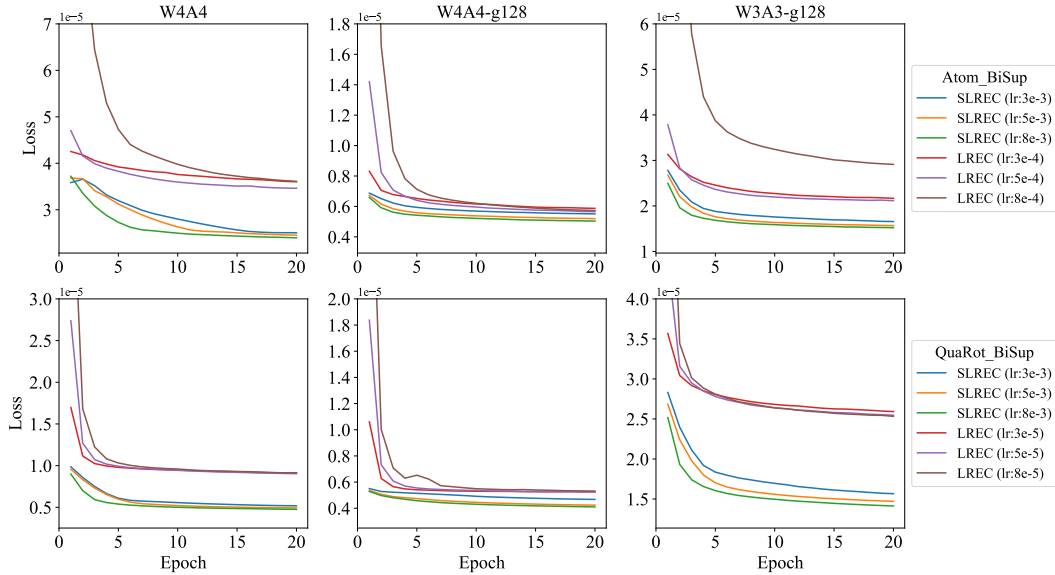


Figure A1: Loss curves on the first layer of Llama3-8B under different settings. (S)LREC denotes (Stabilized) Low-Rank Error Compensation.

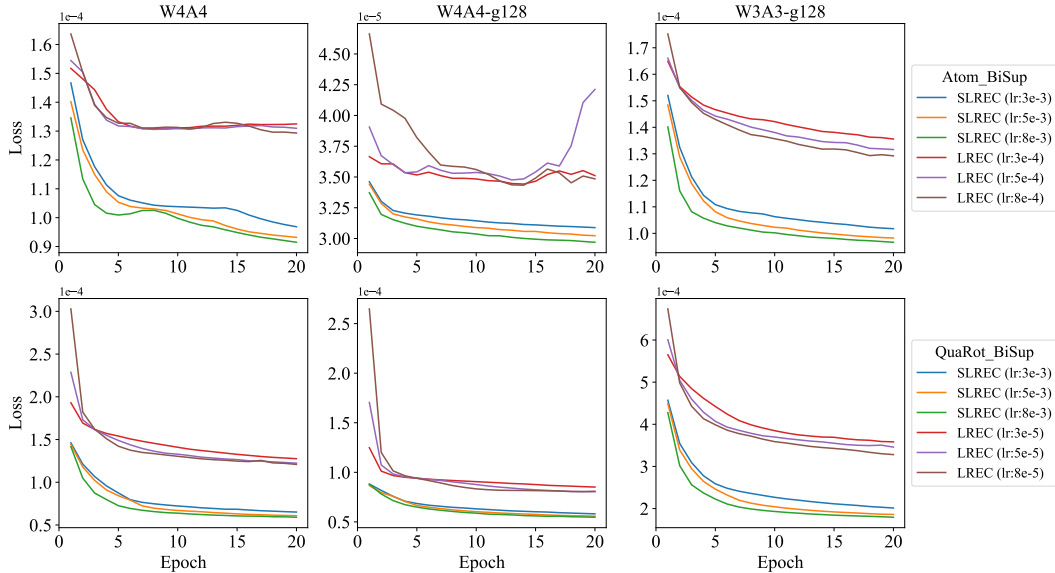


Figure A2: Loss curves on the first layer of Qwen1.5-7B under different settings. (S)LREC denotes (Stabilized) Low-Rank Error Compensation.

In order to verify the effectiveness of the modifications on the proposed techniques, we conducted comparative experiments with their original versions. Specifically, the Weight-Activation Clipping uses the same clip value for the entire tensor (§4.1), the Weight-Activation Smoothing employs the same smoothing factor for weight and activation (§4.2), and the Low-Rank Error Compensation adopts the form similar to LoRA (§4.3). The results of clipping and smoothing techniques are presented in Table A11. It can be seen that FWAC always outperforms WAC, while SWAS outperforms WAS in most cases, suggesting the validity of the modifications and that different combinations of

Table A11: WikiText2 perplexity results of Llama-3-8B with different techniques. The notations are explained as follows: (F)WAC denotes (Fine-grained) Weight-Activation Clipping and (S)WAS means (Soft-constrained) Weight-Activation Smoothing.

Llama-3-8B / PPL↓	W4A4	W4A4-g128	W3A3-g128
Atom (RTN)	50.19	7.78	223.76
Atom (RTN) + WAC	25.39	8.44	83.40
Atom (RTN) + FWAC	25.39	8.21	50.29
Atom (RTN) + FWAC + WAS	15.21	7.80	34.94
Atom (RTN) + FWAC + SWAS	20.03	7.77	34.91
QuaRot (RTN)	19.08	9.28	4138.60
QuaRot (RTN) + WAC	10.03	8.82	218.19
QuaRot (RTN) + FWAC	10.03	8.12	174.81
QuaRot (RTN) + FWAC + WAS	8.15	7.56	204.91
QuaRot (RTN) + FWAC + SWAS	8.13	7.41	21.43

techniques may be required for different settings. As depicted in Figures A1 and A2, compared to LREC, SLREC achieves better convergence and does not require choosing different learning rates for different settings to obtain stable performance, verifying the effectiveness of the proposed improvement.

A.4 Hyperparameter Studies

Table A12: WikiText2 perplexity results of Llama-3-8B with different Samples and Iterations.

Llama-3-8B / PPL↓	S	Atom_BiSup			QuaRot_BiSup			
		I	5	10	20	5	10	20
W4A4	64		22.86	16.08	14.05	7.84	7.41	7.33
	128		16.32	14.53	13.46	7.42	7.30	7.27
	256		14.61	13.84	13.21	7.32	7.30	7.28
W4A4-g128	64		7.62	7.53	7.48	7.13	7.09	7.08
	128		7.55	7.50	7.47	7.11	7.07	7.08
	256		7.48	7.44	7.42	7.07	7.08	7.06
W3A3-g128	64		22.79	17.37	15.72	16.18	13.37	12.28
	128		18.68	16.03	14.97	13.69	12.42	11.82
	256		16.58	15.07	14.43	12.65	12.10	11.63

Table A13: WikiText2 perplexity results of Llama-3-8B with different Rank.

Llama-3-8B / PPL↓	Atom_BiSup			QuaRot_BiSup		
	16	32	64	16	32	64
W4A4	16.81	16.32	16.07	7.44	7.42	7.39
W4A4-g128	7.56	7.55	7.51	7.10	7.11	7.07
W3A3-g128	19.38	18.68	17.88	13.91	13.69	13.33

Experience has shown that algorithms based on gradient optimization are sensitive to the choice of hyperparameters. In this section, we conduct experiments on the main hyperparameters of BiSup, which are directly linked to the overhead of fine-tuning, including the number of training **samples**, the number of fine-tuning **iterations**, and the **rank** of the low-rank error compensation matrix. The results are shown in Tables A12 and A13. Generally speaking, BiSup can produce better results with more samples, larger iterations, and higher rank. However, the required memory footprint and computation time increase accordingly, as illustrated in Table A14. In our experiments, we use 128 samples to fine-tune 5 iterations with a rank of 32. Obviously, the results produced in this configuration do not represent the optimal results for BiSup. Since our aim is to verify the general validity of BiSup, relatively simple configurations are chosen for a wide range of experiments, which can significantly reduce the cost of the experiments and have no impact on the main conclusions.

Table A14: The memory footprint and quantization time of Llama models in W4A4-g128.

Samples - Iterations - Rank		Atom_BiSup			QuaRot_BiSup		
		1-30B	2-13B	3-8B	1-30B	2-13B	3-8B
64 - 5 - 32	Time (min)	74	32	17	71	32	17
	Memory (MiB)	18,414	13,684	10,192	16,388	12,094	9,372
128 - 5 - 32	Time (min)	148	62	34	141	59	34
	Memory (MiB)	22,126	17,012	12,262	19,716	15,422	11,420
128 - 10 - 32	Time (min)	285	120	66	270	114	63
	Memory (MiB)	22,126	17,012	12,262	19,716	15,422	11,420
128 - 10 - 64	Time (min)	285	120	66	270	114	63
	Memory (MiB)	22,146	17,016	12,260	19,736	15,426	11,420